Induction welding and heat treatment of steel pipes: evolution of crystallographic texture detrimental to toughness

P. Yan*[1], Ö. E. Güngör[2], P. Thibaux[2] and H. K. D. H. Bhadeshia[1]

Steel welding using induction heating to produce pipelines is found to have lower toughness at the weld junction than the base material, even after a heat treatment which reaustenitises the weld zone. Detailed crystallographic characterisation indicates that the poor toughness is due to the crystallographically coarse grains present after welding; the coarse scale is not visible using just optical microscopy. The post-weld heat treatment does not improve the situation at the weld junction, because the detrimental crystallographic characteristics are reproduced on cooling.

Keywords: Steel, Pipeline, Induction welding, Toughness, Crystallography

Introduction

High frequency induction heating is often used for brazing difficult alloys of iron[1,2] and for the welding of steel pipes.[3–5] This process enables high productivity in manufacturing pipes with different dimensions, without using any welding consumables.[6] The classical X60, X65 and X70 linepipe steels[7–9] can, by using induction welding, be manufactured into pipes of 18 m in length, 0·5 m in diameter and 13 mm in thickness, for further connection into long distance conduits for natural gas or oil.[10] An important parameter in ensuring the structural integrity of welded pipes which serve in difficult environments is toughness, which must be adequate across all of the zones influenced by the welding.[11–16]

In this work, the authors investigate a pipe induction welding process in which a narrow central zone with a coarse microstructure is formed at the weld junction. There is no external cooling exerted on the pipe after welding; cooling of the welds before heat treatment is mainly due to the conduction between the narrow heated region and the rest of the pipe. To refine the resulting coarse microstructure, the welding is followed by cooling to room temperature and then by an induction heat treatment where the steel locally achieves a fully austenitic state at the peak temperature. The Ae_3 temperature of a typical X65 steel grade X65 is around 880°C.[8,17] The peak temperature in this heat treatment is set well above Ae_3 given the very high rate associated with induction heating, typically 100°C s^{-1}.

Although the toughness of the welded region improves as a consequence of this treatment, the increase is not as large as might be expected from the reduction in the scale of the final microstructure, as is evident in Fig. 1, particularly at the location of the weld junction. One possibility is that although the optical microstructure is refined by the heat treatment, the crystallographic grain size is not.[18–21] The purpose of the present work was to investigate this scenario using the electron backscatter diffraction (EBSD) technique.[22–25]

Experimental procedure

The steel, which falls into the X65 category, has a chemical composition of Fe–0·041C–1·1Mn–0·18Si–0·032Al–0·0053N, microalloyed with Nb and V. The pipe was seam welded in a solid state induction process in which the butting edges of the pipe are pushed together while they are hot and plastic, thus giving rise to flow which expels undesirable oxides from the weld, and at the same time leads to a metallurgical bond by breaking the interfaces between the edges. After welding, it is induction heat treated. Details of the heat treatment are proprietary, but it involves rapid heating to above a temperature at which austenite can form, and subsequent fast cooling. Specimens were obtained before and after the post-welding heat treatment. All the samples were cut normal to the welding direction which is parallel to the rolling direction, which in turn is parallel to the pipe axis. Samples were then ground using sand paper, polished with diamond paste and finally finished using colloidal silica. The sample surfaces for analysis are illustrated in Fig. 2.

A Camscan MX2600 scanning electron microscope equipped with a field emission gun and an EBSD system was used in conjunction with HKL Channel 5 software. The orientation images were taken at an operating voltage of 25 kV, a working distance of 30 mm and a tilt angle of 70°. EBSD scans were conducted using a step size of 0·2 μm. All the pole figures reported here are equal area stereographic projections.

A Philips PW1820 X-ray diffraction goniometer with Cu K_α=1·5406 Å radiation was used for continuous scanning with scan step time of 12·5 s at the step size of 2θ=0·05° on the weld junction.

[1]Department of Materials Science and Metallurgy, University of Cambridge, Pembroke Street, Cambridge CB2 3QZ, UK
[2]ArcelorMittal R&D Industry Gent, OCAS NV, Pres. J. F. Kennedylaan 3, BE-9060 Zelzate, Belgium

*Corresponding author, email py210@cam.ac.uk

Published by Maney on behalf of the Institute
Received 8 September 2009; accepted 28 October 2009
DOI 10.1179/136217109X12568132624163

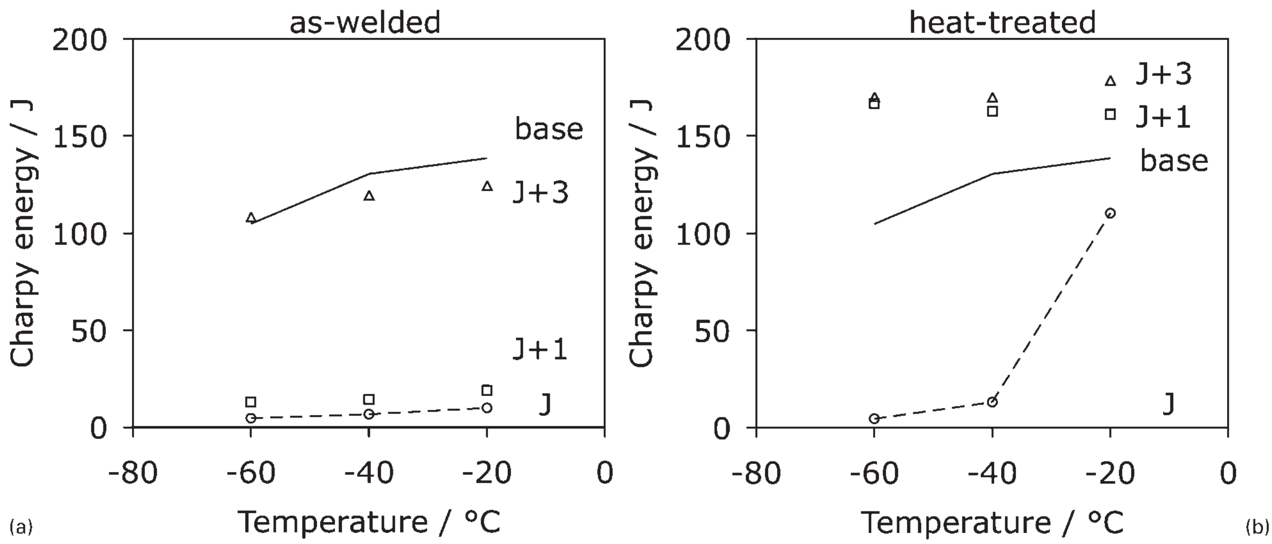

a as welded condition; *b* welded and heat treated

1 **Charpy impact test energy as function of temperature:[18] 'J' designates weld junction, and when used on its own, Charpy notch is located at fusion surface; 'J+1' represents case where notch is 1 mm away from junction**

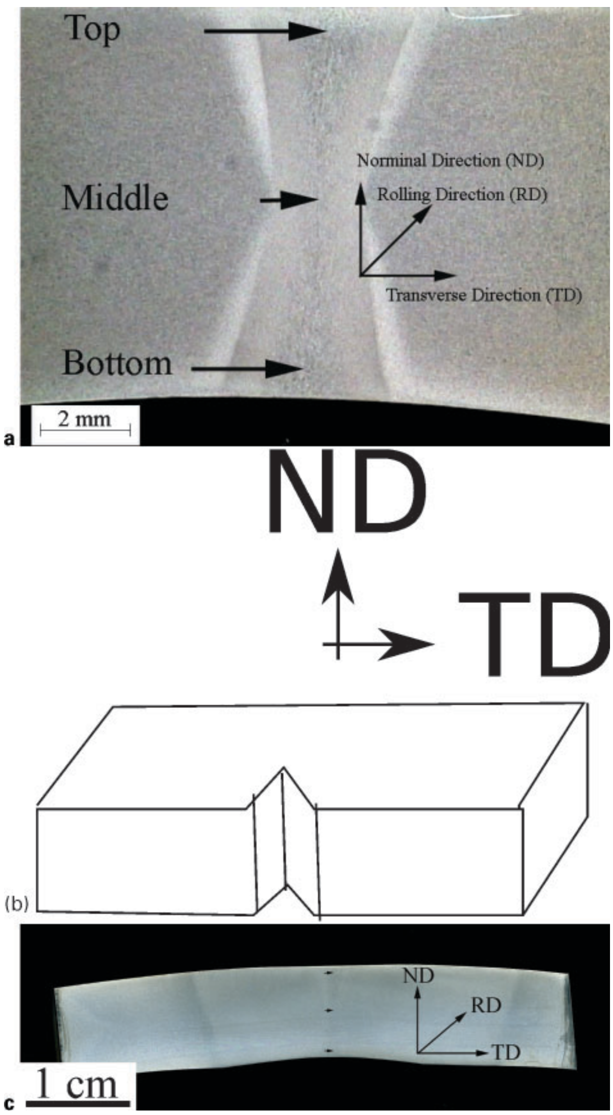

2 ***a*** **orientation of as welded sample relative to steel processing directions: top and bottom line is near outer and inner surfaces of pipe respectively, while middle line is in mid-thickness of pipe,** ***b*** **orientation of Charpy specimen and** ***c*** **joint segment after post-welding heat treatment**

Cross-weld microhardness measurements were carried out on an as welded sample and the sample after post-welding heat treatment using a Mitutoyo microhardness tester with a load of 200 gF and dwell time of 10 s. The microhardness was measured at every 150 μm interval.

Results and discussion

The distributions of microhardness of the as welded sample and heat treated sample are shown in Fig. 3 respectively. The origin of the X-axis corresponds to the centre of the weld junction. After post-welding heat treatment, hardness is more uniformly distributed across the weld.

It is noted here that as expected from the lean chemical composition of the steel, retained austenite was not confidently detected in the final weld by EBSD scanning using a small step size of 200 nm. The X-ray diffraction patterns in Fig. 4 confirm the absence of a detectable quantity of austenite.

The induction welding process involves the upsetting of the two parts being joined in order to expel a certain amount of steel; this helps make a clean joint free from inclusions. Nevertheless, the possibility of oxides at the weld junction was investigated using extensive optical and scanning electron microscopy. These experiments did not reveal any role of inclusions in determining the impact properties at the junction. Broken Charpy samples from the weld junction were also examined because there is a better chance of detecting significant initiating features, but this led to the same conclusion. A typical fracture surface of the sample after post-weld heat treatment, failed at the weld junction at $-40°C$, is shown in Fig. 5. Indeed, the fractography was not particularly different when compared with samples far from the weld junction when the comparisons were made for the same quasi-cleavage mode.

Figure 6 shows a ferrite orientation image from a region 3 mm away from the weld junction, i.e. with crystal orientations unaffected by the welding process. The steel is textured, as illustrated by the {100} pole figure. However, when the pole figure is constructed for a region ~ 20 mm^2, corresponding to the size of typical

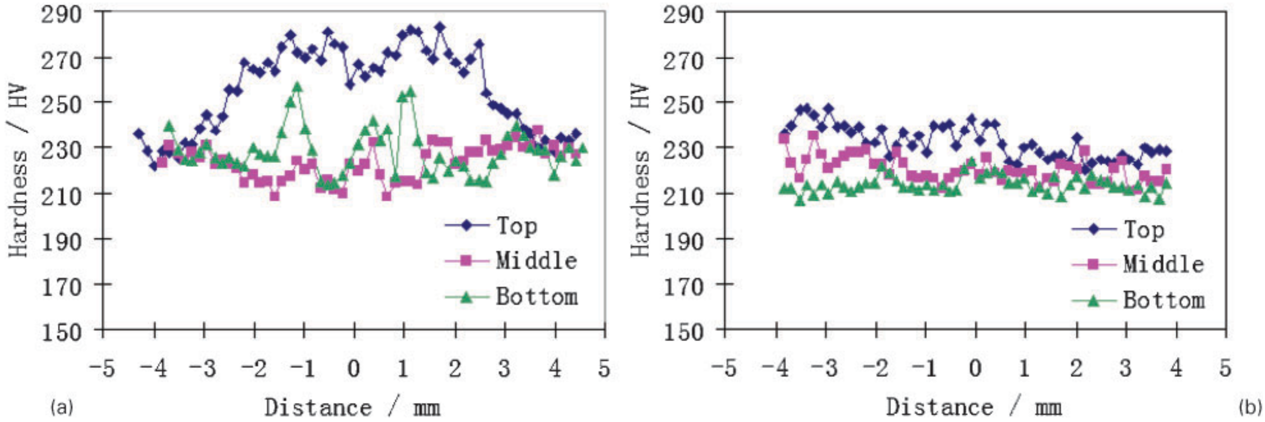

a **as welded condition;** ***b*** **welded and heat treated**
3 Cross-weld microhardness measurements

fracture facets on low temperature Charpy tests,[18] it is clear that there the ferrite grains within this region have a large range of orientations. Since one of the important factors influencing the absorption of energy during cleavage fracture is the deflection of propagating cracks across grain boundaries, such a texture bodes well for toughness, consistent with the baseplate data illustrated in Fig. 1.

The situation changes dramatically in the affected regions of the weld. Figure 7 shows the ferrite crystal orientations as a function of the distance from the weld junction, with the scan conducted along the bottom of the joint, i.e. near the inner surface of the pipe (Fig. 2*a*). The coarse crystallographic grain size in the vicinity of the weld junction is apparent from the large clusters of grains which have a similar colour coding. The overall texture both in the region 1 mm away from the junction and in its close proximity is much sharper (cf. Figs. 6*b* and 7*b*). The coarse crystallographic grain size accounts for the poor toughness recorded from Charpy tests[20] of as welded samples conducted on these regions (Fig. 1).

The results from the sample post-weld heat treated are presented in Fig. 8. Bearing in mind that the weld region becomes fully austenitic and then is cooled to ambient temperature, it might be expected that the microstructure refines and achieves better mechanical properties. Although at first glance, the refinement may appear to have happened, the crystallographic data indicate otherwise. The texture in the region (i) $\sim$1 mm from the junction has weakened relative to the as welded state, and hence the considerably improved Charpy energies (Fig. 1*b*). However, the region adjacent to the weld region (ii) still exhibits a strong texture, and the typical result illustrated for region (iii) indicates that the orientation differences between the grains within the 20 μm interval regions are very small. Hence, the post-weld heat treatment does not result in an improvement of the low temperature Charpy energy (Fig. 1*b*).

The {100} plane is the cleavage plane of BCC iron crystal,[26,27] so a high density of {100} planes parallel to rolling direction should lead to a lower fracture energy. It is useful therefore to examine the distribution of {100} planes relative to the geometry of the Charpy test. The V notches of the samples were consistent with standard industrial practice, machined to be parallel to the rolling direction. It is relevant that Fig. 9 shows the distribution of {100} poles relative to the transverse direction (which is normal to the mean fracture plane of the Charpy specimen). A high density of poles parallel to the transverse direction implies a polycrystallography which is conducive to cleavage crack propagation.

The weld junction, both before and after the heat treatment, retains the highest density of cleavage planes in an unfavourable orientation, which is consistent with the failure to improve toughness following reaustenitisation of the welded region. The observed densities are much higher than for the region 3 mm away from the junction, i.e. the plate which is crystallographically unaffected by the weld. The region 1 mm from the junction has a generally low density of {100} poles

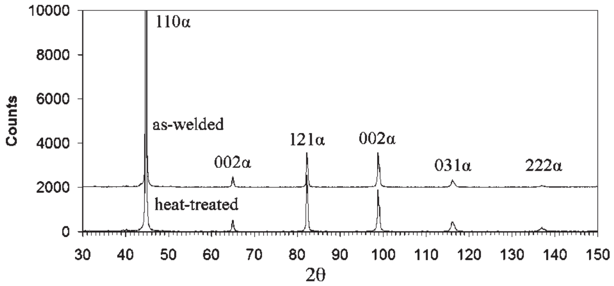

4 X-ray diffraction pattern for as welded sample and welded and heat treated sample: Bragg angle is designated θ in degrees

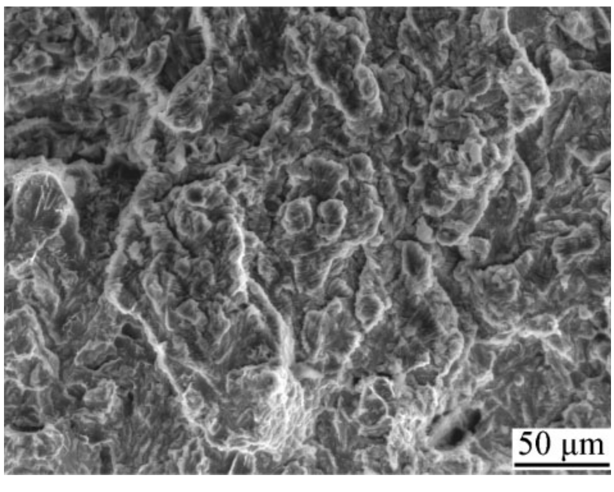

5 Fracture surface at weld junction after post-weld heat treatment, tested at −40°C

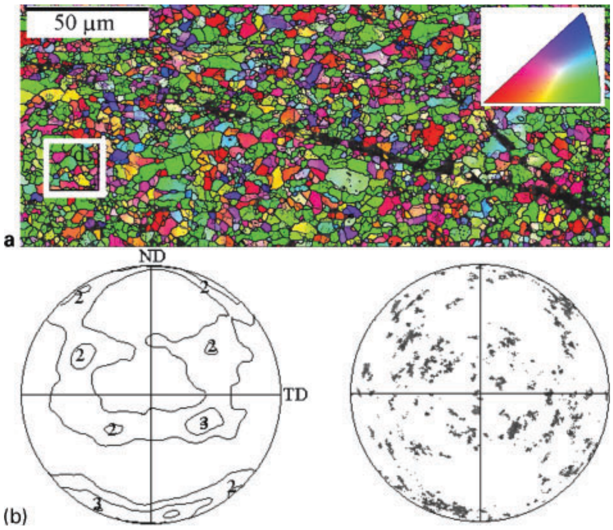

6 ***a*** **orientation image of unaffected area, 3 mm away from weld junction, and** ***b*** **{100} pole figure on left is for full area illustrated, whereas that on right is for boxed region in** ***a***

parallel to the transverse direction, so the plot in Fig. 9 does not explain why its toughness is poor in the as welded condition, other than due to the fact that its crystallographic grain size is large in the as welded condition, as is clear from region (i) in Fig. 7, where significant areas with uniform colours are seen. As Fig. 8 shows, the texture 1 mm from the junction weakens on heat treatment.

Further analysis has been conducted in order to confirm the role of crystallography in the cleavage fracture process. Strings of grains (defined as those with misorientations across grain boundaries which are greater than 2°) in the close proximity of the −40°C fracture at the weld junction were analysed to examine approximately the continuity of {100} planes across

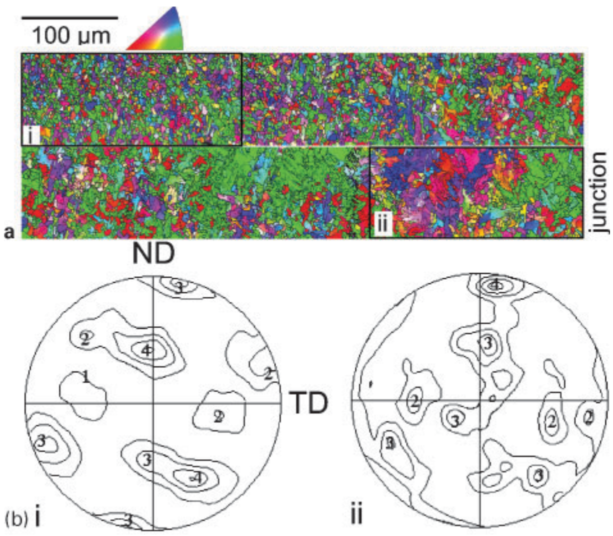

7 ***a*** **orientation image along bottom line of as welded sample: scan begins at top left and continues towards weld junction from bottom left, and** ***b*** **{100} pole figures from regions marked 'i' and 'ii', showing texture in region 1 mm from junction and in close vicinity of junction**

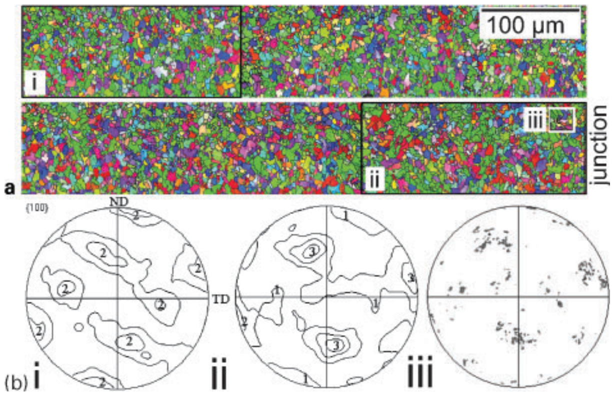

8 ***a*** **orientation image along bottom line of weld after post-weld heat treatment: region marked iii is enclosed in box with white border, and** ***b*** **{100} pole figures of three corresponding regions in** ***a***

grains. For comparison purposes, a similar string from a region 3 mm from the junction was also studied; the sample in this case was unbroken to avoid the plastic deformation due to the high toughness of this area (Fig. 10).

The analysis is approximate because the edge to edge matching of cleavage planes between adjacent grains is not considered, but rather is based on the overall angle between planes from neighbouring crystals. The cleavage crack propagates linearly along effective grains, and is deviated at boundaries between effective grains, which was also pointed out in Ref. 28. Figure 11 shows that the weld junction compares unfavourably relative to the unaffected baseplate since large cleavage facets are expected.

Summary

It appears that the poor toughness of the region of an induction weld which is close to the weld junction is substantially related to the crystallographically coarse grains present there after welding. Reaustenitisation of the affected regions does not improve the situation at the weld junction, because the detrimental crystallographic characteristics are reproduced on cooling. Studies need to be conducted on heat treatments which eliminate these textures and produce a more random set of ferrite orientations in the weld affected regions.

Acknowledgements

The authors are grateful to ArcelorMittal for financial and technical support, and would like to thank E. Hivert

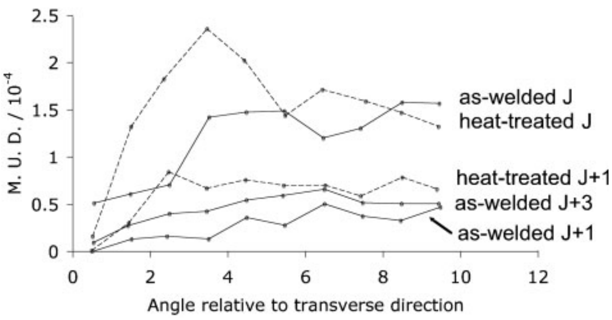

9 Plot of multiple of uniform density (M. U. D.) for angle in degrees, made by {100} poles to transverse direction

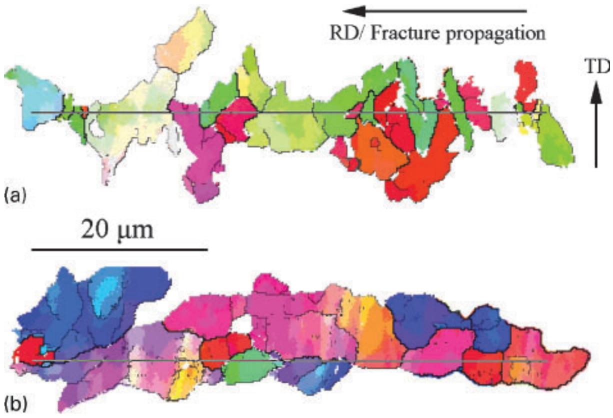

10 Orientation images of grains for calculation of cleavage plane propagation on *a* fractured sample after post-welding heat treatment and *b* base metal of as welded sample

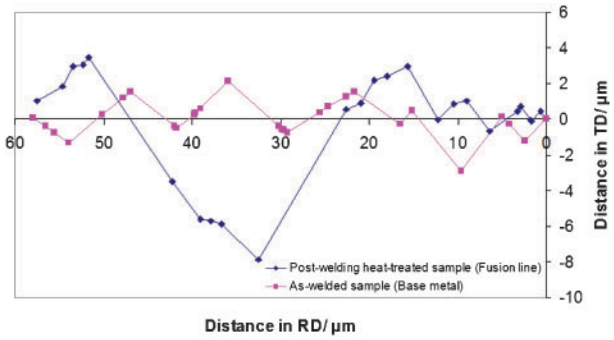

11 Calculated cleavage plane propagation curves

and D. Quidort from ArcelorMittal for helpful discussions. They also thank Professor A. L. Greer for the provision of laboratory facilities at the University of Cambridge.

References

1. D. Durand, D. Coupard, C. Goetz and F. Girot: 'Determination of optimal brazing frequency by solution of thermal and electromagnetic models', *Sci. Technol. Weld. Join.*, 2001, **6**, 177–181.
2. K. Saida, B. Jeong and K. Nishimoto: 'Development of hyper-interfacial bonding technique for ultra-fine grained steels and microstructural analysis of bonded joints', *Sci. Technol. Weld. Join.*, 2004, **9**, 548–554.
3. E. Mikami, Y. Shirakawa, K. Fujimoto, J. Hamaguchi and I. Yasamura: 'Development of new hot-welded steel pipe-making process', *ISIJ Int.*, 1991, **31**, 635–639.
4. K. D. Houghton: 'Welded linepipe for offshore sour service applications', *J. Offshore Technol.*, 1995, **3**, 46–48.
5. H.-J. Kim and S.-K. Youn: 'Three dimensional analysis of high frequency induction welding of steel pipes with impeder', *J. Manuf. Sci. Eng.*, 2008, **130**, 0310051–0310057.
6. AWS: 'High frequency welding', in 'Welding handbook', 156; 1982, Miami, FL, AWS.
7. C. Shiga, A. Kamada, T. Hatomura, K. Hirose, J. Junichi and T. Sekine: 'Development of large diagmeter high strength line pipes for low temperature services', Technical report 4, Kawasaki Steel Technical Report, 97–109, Kawasaki Steel, Tokyo, Japan, 1981.
8. J. Q. Wang, A. Atrens, D. R. Cousens and N. Kinaev: 'Microstructure of X52 and X65 pipeline steels', *J. Mater. Sci.*, 1999, **34**, 1721–1728.
9. M. C. Zhao, K. Yang, F. R. Xiao and Y. Y. Shan: 'Continuous cooling transformation of undeformed and deformed low carbon pipeline steels', *Mater. Sci. Eng. A*, 2003, **A355**, 126–136.
10. E. Treiss: 'Induction annealing of welds in the fabrication of high-frequency induction welded steel line pipes', *3R Int.*, 1981, **20**, (11), 627–630.
11. J. G. Williams, C. R. Killmore, F. J. Barbaro, J. Piper and Fletcher: 'High strength erw linepipe manufacture in australia', *Mater. Forum*, 1996, **20**, 13–28.
12. N. Pradhan, N. Banerjee, B. B. Reddy, S. K. Sahay, D. S. Basu, P. K. Bhor, S. Das and S. Bhattyacharya: 'Control of defects during continuous casting of line pipe (API) quality steels', *Scand. J. Metall.*, 2005, **34**, 232–240.
13. C. Yu: 'Metallographic examination evaluation criteria and control for ERW pipe production', *Tube Int.*, Mar. 1996, 153–155.
14. G. Thewlis: 'Weldability of X100 linepipe', *Sci. Technol. Weld. Join.*, 2000, **5**, 365–377.
15. K. Faes, A. Dhooge, P. de Baet and P. Afschrift: 'Influence of deceleration phase on properties of friction welded pipelines using intermediate ring', *Sci. Technol. Weld. Join.*, 2008, **13**, 136–145.
16. G. Magudeeswaran, V. Balasubramanian, T. S. Balasubramanian and G. M. Reddy: 'Effect of welding consumables on tensile and impact properties of shielded metal arc welded high strength, quenched and tempered steel joints', *Sci. Technol. Weld. Join.*, 2008, **13**, 97–105.
17. M. Militzer, R. Pandi and E. B. Hawbolt: 'Ferrite nucleation and grouth during continuous cooling', *Metall. Trans. A*, 1996, **27A**, 1547–1556.
18. P. Yan, Ö. E. Güngör, P. Thibaux and H. K. D. H. Bhadeshia: 'Induction-welded and heat-treated pipeline steel', *Adv. Mater. Res.*, 2010, 651–656.
19. A. Lambert-Perlade, A. F. Gourgues and A. Pineau: 'Austenite to bainite phase transformation in the heat-affected zone of a high strength low alloy steel', *Acta Mater.*, 2004, **52**, 2337–2348.
20. D. Bhattacharjee, J. F. Knott and C. L. Davis: 'Charpy-impact-toughness prediction using an 'effective' grain size for thermo-mechanically controlled rolled microalloyed steels', *Metall. Mater. Trans. A*, 2004, **35A**, 121–130.
21. Y. M. Kim, S. Y. Shin, H. Lee, B. Wang, S. Lee and N. J. Kim: 'Effects of molybdenum and vanadium addition on tensile and charpy impact properties of API X70 linepipe steels', *Metall. Mater. Trans. A*, 2007, **38A**, 1731–1742.
22. D. J. Dingley and M. M. Nowell: 'The use of electron backscatter diffraction for the investigation of nano crystalline materials and the move towards orientation imaging in the TEM', *Microchim. Acta*, 2004, **147**, 157–165.
23. F. J. Humphreys: 'Characterisation of fine-scale microstructures by electron backscatter diffraction (EBSD)', *Scr. Mater.*, 2004, **51**, 771–776.
24. A. F. Gourgues-Lorenzon: 'Application of electron backscatter diffraction to the study of phase transformations', *Int. Mater. Rev.*, 2007, **52**, 65–128.
25. L. Mujica, S. Weber, C. Thomy and F. Vollertsen: 'Microstructure and mechanical properties of laser welded austenitic high manganese steels', *Sci. Technol. Weld. Join.*, 2009, **14**, 517–522.
26. W. R. Tyson, R. A. Ayres and D. F. Stein: 'Anisotropy of cleavage in BCC transition metals', *Acta Metall.*, 1973, **21**, 621–627.
27. V. M. Goritskii and D. P. Khromov: 'Crystallographic direction of brittle transcrystalline cleavage in the ferrite of low-carbon low-alloy steels', *Probl. Proch.*, 1984, **6**, 81–82.
28. S. Y. Shin, S. Y. Han, B. Hwang, C. G. Lee and S. Lee: 'Effects of Cu and B addition on microstructure and mechanical properties of high-strength bainitic steels', *Mater. Sci. Eng. A*, 2009, **A517**, 212–218.